EJC Paediatric Oncology 4 (2024) 100185

Contents lists available at ScienceDirect

EJC Paediatric Oncology

journal homepage: www.journals.elsevier.com/ejc-paediatric-oncology

Multimodality imaging of bone marrow involvement in paediatric oncology

Rutger A.J. Nievelstein [a,*], Lise Borgwardt [b], Thekla von Kalle [c], Annemieke S. Littooij [a], Lil-Sofie Ording Müller [d], Nelleke Tolboom [a]

[a] Department of Radiology & Nuclear Medicine, UMC Utrecht/Wilhelmina Children's Hospital, and Princess Máxima Center for Pediatric Oncology, Utrecht, the Netherlands
[b] Department of Clinical Physiology and Nuclear medicine, Copenhagen University Hospital, Rigshospitalet, Copenhagen, Denmark
[c] Radiological Institute Olgahospital, Klinikum Stuttgart, Stuttgart, Germany
[d] Division of Radiology and Nuclear Medicine, Oslo University Hospital, Oslo, Norway

ARTICLE INFO

Keywords:
Multimodality imaging
Paediatric radiology
MRI
PET
Bone marrow
Bone marrow involvement
Metastases
Paediatric oncology
Children
Nuclear Medicine
PET/CT

ABSTRACT

Identifying bone marrow involvement (with or without bone destruction) in children with cancer is essential for adequate diagnosis, prognostication, therapy planning, and response assessment. Imaging plays an increasing role, with MRI including DWI and [^{18}F]FDG-PET/CT as the most commonly used imaging techniques. Interpretation of the paediatric bone marrow on imaging might be challenging because of age-related physiological changes in the bone marrow, as well as disease and therapy related effects. In this review, we discuss how the imaging techniques available may be employed to detect bone marrow involvement (BMI) in paediatric oncology. Furthermore, insights into physiological, disease and therapy related bone marrow changes in children that might influence bone marrow imaging interpretation will be provided.

1. Introduction

The bone marrow is one of the largest and most dynamic organs in the paediatric body, frequently involved in paediatric oncological diseases. This not only includes metastatic involvement but also primary neoplastic disorders, as well as other disease and treatment related secondary changes. Interpretation of these bone marrow abnormalities on imaging may be challenging as normal physiological changes during childhood and adolescence do occur. Several imaging techniques are nowadays used to noninvasively investigate and characterize bone marrow diseases in children. Conventional (whole body) magnetic resonance imaging (MRI) is often the first imaging modality of choice in bone marrow imaging. To increase the specificity, other imaging techniques, including focused diffusion weighted imaging (DWI), chemical shift imaging (CSI), and dynamic contrast-enhanced MRI (DCE-MRI), as well as spectral computed tomography (CT), and nuclear medicine techniques such as Positron Emission Tomography (PET), are increasingly applied.

In this review, we will provide an overview of the imaging techniques available to study the bone marrow with their strengths and limitations. The normal appearances of bone marrow in children will be discussed followed by general and tumour type specific presentations of bone marrow involvement (BMI) in paediatric oncology. Finally, treatment related bone marrow changes will be described and how they can be distinguished from active disease.

2. Imaging techniques

2.1. Magnetic resonance imaging (MRI) [1–6]

2.1.1. Conventional MRI

MRI is the imaging modality of first choice to investigate the bone marrow. It allows imaging of the bone marrow directly with the excellent spatial and contrast resolution necessary to differentiate the MRI signal intensities of the different marrow elements and pathologies. Due to the different amount of fat and water, yellow and red marrow will show different signal intensities on the various MRI sequences used, which will be discussed in more detail later. A basic bone marrow

* Correspondence to: Department of Radiology & Nuclear Medicine, Division Imaging & Oncology, UMC Utrecht/Wilhelmina Children's Hospital, P.O. Box 85500, Utrecht, GA 3508, the Netherlands.
E-mail address: r.a.j.nievelstein@umcutrecht.nl (R.A.J. Nievelstein).

https://doi.org/10.1016/j.ejcped.2024.100185
Received 30 April 2024; Received in revised form 30 July 2024; Accepted 3 August 2024
Available online 13 August 2024

imaging protocol usually consists of T1-weighted (T1w) and T2-weighted (T2w) turbo spin echo (TSE) sequences, the latter should be combined with a fat suppression technique to improve the differences in signal intensities of the bone marrow elements and pathologies. The most common fat saturation techniques used are Short Tau Inversion Recovery (STIR), Spectral Attenuated Inversion Recovery (SPAIR) and the Dixon method. STIR has the advantage that it is relatively insensitive to magnetic field inhomogeneities whereas the Dixon method is faster and provides a higher signal-to-noise ratio. The Dixon method is an example of *chemical-shift imaging (CSI)* that relies on the slight difference in resonance frequency between fat and water within the magnetic field generating so called in-phase and opposed-phase images which may be useful in differentiating tumour from normal bone marrow. In addition, by using postprocessing tools, fat-only and water-only images can be reconstructed and quantification of the amount of fat within tissues or lesions is possible. Recent studies indicate that the T2 Dixon fat images may replace the T1w TSE sequence in the basic protocol for bone marrow imaging, which reduces scan time without loss of information [7,8]. The most important disadvantages of the Dixon method include its sensitivity to metal artefacts and main magnetic field inhomogeneities, and the risk of fat-water swapping artefacts [9]. The latter occurs when there is a misregistration of the fat and water images due to motion or other factors during the image acquisition. This can lead to incorrect fat-water separation which will affect image quality, potentially resulting in misinterpretation of the tissue composition.

2.1.2. *Diffusion weighted imaging (DWI) [10,11]*

DWI is based on the measurement of random Brownian motion of water protons within tissues, which is influenced by the microscopic structure and organization of these tissues. The signal intensity on DWI reflects the rate of intra-, extra-, and transcellular motion of water protons within a voxel. For instance, in tumours with high cellularity, the water movement will be decreased due to a relative decrease in intra- and extracellular volume. Besides these tissue or pathology related factors, the DWI signal is also influenced by technical factors such as the pulse sequence chosen, and the strength of diffusion weighting given by the b-value. If two or more b-values are used, semi quantification of the diffusion becomes possible in the form of an apparent diffusion coefficient (ADC), which is therefore recommended. Although DWI can be helpful in lesion detection and treatment response assessment, it must be used with caution in infants and young children, as (cell rich) red marrow also restricts diffusion [12].

2.1.3. *Contrast-enhanced MRI (CE-MRI)*

Both normal red bone marrow and several bone marrow pathologies do show enhancement after intravenous administration of gadolinium, but the degree of enhancement varies greatly. It not only depends on physiologic changes seen in children but also on technical factors like the magnetic field strength and pulse sequence used. In particular in young children with mainly red bone marrow, CE-MRI is less sensitive in detecting (subtle) bone marrow disease. Therefore, the use of gadolinium is usually not necessary for diagnosis and staging of focal or multifocal BMI.

2.1.4. *Magnetic resonance spectroscopy (MRS)*

With MRS the metabolic profile of tissues can be measured. Although some studies in adults suggest that it can be used to discriminate malignant from benign bone marrow lesions, its use in the skeletal system is limited. This is mainly due to the signal drop out from cortical bone and spectral peak contamination from adipose tissues.

2.2. *Spectral computed tomography (CT) [5,6,13]*

Spectral CT (also called dual-energy or multi-energy CT) consists of the acquisition of CT measurements at two or more X-ray energy levels. This allows for characterization and quantification of tissue components and materials since they will have different attenuation characteristics at different X-ray energies. Examples of its use are the detection of bone marrow lesions or bone marrow oedema by subtracting the mineralized bone tissue from the image (so called virtual non-calcium (VNCa) images). Although promising, its role in paediatric bone marrow imaging has yet to be established.

2.3. *Nuclear medicine imaging [14]*

Several nuclear medicine imaging techniques can be used to investigate the physiological bone and bone marrow, with various indications. From an oncological perspective, BMI is usually assessed using the generic positron emission tomography (PET) tracer ^{18}F-fluorodeoxyglucose ([^{18}F]FDG). Additionally, disease specific tracers such as ^{123}Iodine-labeled metaiodobenzylguanidine ([123I]mIBG) or ^{68}Gallium-labeled DOTATATE ([^{68}Ga]DOTATATE) for neuroblastoma can visualize BMI. These disease specific tracers will be discussed in the appropriate sections in the manuscript.

2.3.1. *[^{18}F]FDG-PET*

[^{18}F]FDG-PET is widely used in the evaluation of oncological disease. It is combined with a low dose CT of the body without intravenous (iv) contrast material administration for attenuation correction and anatomical mapping but can also be combined with a diagnostic CT after iv contrast material administration if clinically indicated. [^{18}F]FDG uptake is a measure of cell glucose use and therefore cell metabolism. [^{18}F]FDG-PET is metabolically trapped in the cell after phosphorylation as FDG-6-phosphate. Unlike glucose, [^{18}F]FDG-PET does not further participate in the glycolytic pathway and remains in the cell. Use in children with cancer face some practical challenges and is, as always, associated with concerns related to the ionizing radiation used. However, there have been several technical developments in the last decade that largely address these challenges and concerns. With the newest generation PET/CT-scanners, a PET/low dose CT can now be performed with a radiation dose around or even less than the normal background radiation per year, resulting in an increasing role of molecular imaging in paediatric oncology.

2.3.2. *Skeletal scintigraphy*

Due to the low specificity of bone scans and limited sensitivity for bone marrow infiltration, skeletal scintigraphy is no longer the preferred method for the investigation of bone metastases in paediatric oncology staging.

3. Normal bone marrow in children

The bone marrow in children changes with age and differs from that in adults accordingly. In neonates the ossified part of the skeleton is filled with red bone marrow which gradually converts into yellow marrow in a specific age-dependent pattern. The remaining cellular red bone marrow also undergoes changes and becomes more fatty with age (Fig. 1)[1,15].

The skeleton in children is under constant growth and development towards skeletal maturation. Their skeleton is more vascular, it is more elastic and flexible, and the periosteum is more loosely attached to the bone. In addition, the physes, responsible for skeletal growth, are highly cellular. All these factors influence both normal appearances of the bone marrow on imaging but also the response to stress, trauma, and disease.

3.1. *Normal bone marrow on MRI*

On MRI the bone marrow's response to pathological processes most often appear as focal or generally increased high signal on T2w fat suppressed sequences with corresponding low signal on T1w TSE or T2 Dixon fat images. This signal is in most cases non-specific and merely represents increased water content compared to the surrounding bone

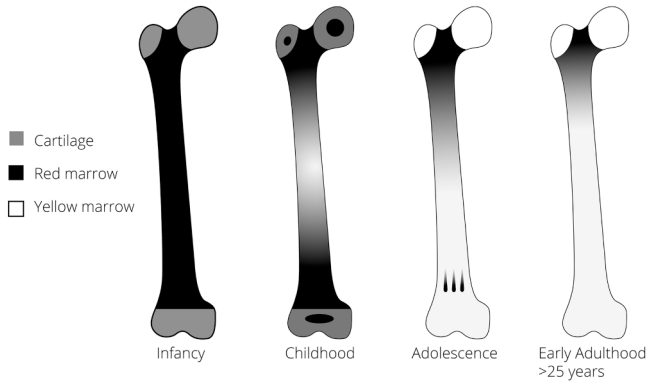

Fig. 1. Normal age-related bone marrow conversion in the long bones. The red to yellow bone marrow conversion occurs in a predictable manner throughout childhood and adolescence, reaching the adult pattern around 25 years of age. The bone marrow conversion starts in the centre of the long bones and progresses proximally and distally toward the metaphysis. In adults residual red bone marrow is confined to the axial skeleton and proximal humeri and femora (reproduced with permission from [16]).

marrow. Research has shown that focal areas of T2 hyperintensity are also frequently seen in the bone marrow of healthy children. These are most often seen in the lower extremities and pelvis, particularly around the knee joint, but also in the hands and can be found in any part of the bone marrow, frequently in an asymmetrical pattern. Soft tissue oedema and particularly bone destruction is, however, rarely seen in these normal bone marrow lesions (Fig. 2)[17–20]. It is important to be aware of the most common appearances and spectrum of findings in the normal bone marrow in children, including the MRI-pattern of red-yellow conversion, to be able to spot general cellular marrow infiltration, but also to be able to differentiate most likely normal, harmless findings from potentially malignant disease. However, this can sometimes be

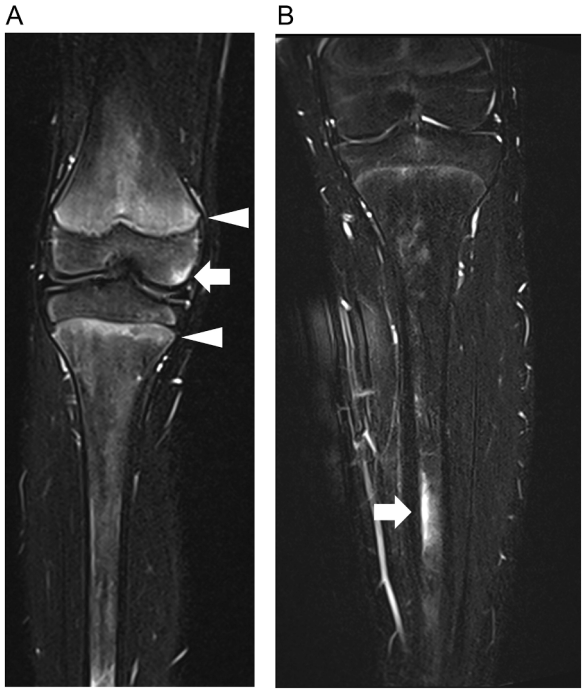

Fig. 2. Coronal MRI Dixon weighted images illustrating areas of normal T2 hyperintensities in the distal epiphysis of the femur (arrow in A), and the diaphysis of the tibia (arrow in B). Please also note the slight T2 hyperintens metaphysis of distal femur and proximal tibia consistent with residual red bone marrow (arrowheads in A).

difficult even for experienced paediatric radiologists. Both diffusion weighted sequences and contrast-enhancement patterns may be of help to increase specificity of the findings, although there is no cut-off ADC-value between malignant and benign lesions [21], and there are no entirely specific contrast enhancement patterns (except for a few entities like bone infarcts). Fat replacement in lesions has been used as a marker for malignancy in adults but there is a paucity of research in children [22]. From personal experience, fat replacement can be seen in benign lesions and malignant lesions, and particularly skeletal manifestations in lymphoproliferative diseases may still contain fat. Therefore, besides the knowledge of normal findings, close clinical-radiological correlation is crucial to guide both detection of disease and further management of equivocal bone marrow findings in children on MRI.

3.2. *Normal bone marrow and growth plates on [^{18}F]FDG-PET*

Physiological [^{18}F]FDG-uptake is seen in the physis (growth plates) of paediatric patients. This uptake differs during different stages of development and corresponds to the age and the site of the physis. The highest [^{18}F]FDG-uptake is seen in the distal femur and looks like a horizontal band of increased uptake in the physes and apophyses. The [^{18}F]FDG-uptake in the physis is usually bilateral and symmetrical (Fig. 3)[23].

In children the red marrow is metabolically active compared to the yellow marrow. It shows an homogenous increase in the [^{18}F]FDG-uptake in the proximal humeri, proximal and distal femora and proximal tibiae, which are sites of red marrow in a growing child. In the non-treated paediatric patient diffuse marrow uptake of [^{18}F]FDG can represent incidental non–treatment-related marrow stimulation, such as the hematopoietic stimulation from anaemia or a systemic inflammatory disease [24]. This is often followed by increased [^{18}F]FDG-uptake of the organs of haematopoiesis and the immune system, including thymus and spleen.

3.3. *Bone marrow involvement – general considerations [1,3–6]*

Malignant BMI in children can represent hematogenous metastases, arise from the myeloid tissue elements (e.g. in haematological malignancies like leukaemia and lymphoma) or from the mesenchymal tissue elements (e.g. in osteosarcoma or Ewing sarcoma). Regarding metastatic disease, terminology is somewhat confusing as both bone metastasis and bone marrow metastasis is used in the literature suggesting that they have a different origin. Historically, this differentiation can probably be explained by the difference between positive bone marrow biopsies versus positive lesions at bone scintigraphy in f.i. lymphomas, which is more about a difference in diffuse versus focal BMI. From a physiological viewpoint, however, all lesions in the bone most likely primarily originate from one of the bone marrow elements instead of the bony components. Consequently, all metastatic lesions in the bone can be regarded as bone marrow metastases, although some will show more bony destruction or osseous matrix than others. However, as discussed further below, this differentiation is still present in several ongoing international research protocols.

On MRI, BMI in children (either metastatic or from myeloid origin) usually presents with low signal intensities on T1w and T2w Dixon fat images, and high signal intensities on T2w images due to the combination of free water and oedema in addition to replacement of the fatty content of normal marrow (Fig. 4A and B)[25]. It can be (multi)focal but is often diffuse, e.g. in leukaemia and neuroblastoma (Fig. 5A and B)[15, 26,27]. In particular in young children it can, however, be very challenging to detect BMI, because the high cellular normal red marrow may show rather similar signal characteristics as BMI, both on T1w and T2w sequences. However, the high T2 signal intensity of normal red marrow is usually less distinct than malignant BMI, best seen on T2w sequences with fat suppression. Furthermore, literature in adults suggests that it

Fig. 3. Coronal whole-body [^{18}F]FDG-PET image in a girl, 17 months of age, illustrating normal [^{18}F]FDG-uptake in the physis (growth plates) at the level of the wrist and knees (arrowheads).

can be helpful to relate the signal intensity of the bone marrow at the T1w sequences with adjacent muscles or vertebral disc, as BMI is usually T1 hypointense compared to muscle and the intervertebral disc, in contrast to normal red bone marrow which is mildly hyperintense relative to muscle [28]. In our experience, however, this "rule" does not always apply in children, both for distinguishing malignant from benign BMI, as well as from normal red bone marrow. Although DWI is widely used for the assessment of adult bone marrow disease, its use in children is more challenging due to the highly cellular hematopoietic marrow that may impede diffusion [12]. A recent study by Rashidi et al. in children and young adults did show, however, that by using both low and high b values, focal bone marrow metastases could be well detected, despite the fact that ADC values could be misleading (Fig. 4C and 5C) [21]. Moreover, DWI should always be used as a complementary sequence to T1w and T2w sequences. Chemical shift imaging (e.g. the Dixon technique) is another sequence that may be used for the assessment of malignant BMI. In case of chemical shift imaging, malignant lesions will most often not demonstrate signal loss on opposed-phase imaging in contrast to normal bone marrow and red bone marrow reconversion, because the vast majority of the malignant lesions do not contain fat [29,30]. However, more research in children is still needed to evaluate the real impact of fat fraction on decision making in malignant BMI. Finally, in adults, the "halo sign" has been described on fluid sensitive (T2w) images as a clue for metastatic disease [31]. It is characterized by a peripheral rim of hyperintensity, which is thought to be the result of focal trabecular destruction and replacement by fluid. Based on our experience, however, this sign is rarely seen in children.

In general, bone marrow activity on [^{18}F]FDG-PET that is more intense than liver activity is considered abnormal (Fig. 4.D and 6). Normal accumulation is generally homogeneous, with a more extensive distribution in children compared with adults [32]. Not all paediatric tumours show [^{18}F]FDG uptake, but in [^{18}F]FDG avid tumours (focal) uptake higher than the liver is considered abnormal. However, it should be kept in mind that increased [^{18}F]FDG uptake is sensitive but not specific, as diffusely increased uptake can also be observed in, for instance, patients with infections, anaemia, and those treated with granulocyte colony-stimulating factor (GCSF)[33]. Moreover, as discussed in the previous section, physiological increase can be seen at the paediatric physis of the growing skeleton. Caution should be taken when [^{18}F]FDG-PET is performed after the start of treatment, as corticosteroids can rapidly and drastically reduce [^{18}F]FDG uptake of the tumour (Fig. 5.D, to be compared with Fig. 6).

As mentioned in the first paragraph, differentiation between bone marrow and bone metastases is a non-physiological differentiation, since it is a spectrum of disease, but because of various ongoing scientific studies a differentiation is still necessary. In these studies, bone metastases are defined by an affection of the bone detected by CT as a lytic lesion or by MRI as an invading lesion in cortical bone or the cancellous bone (spongiosa) at the site of [^{18}F]FDG uptake. If there is no anatomic imaging (low-dose CT, diagnostic CT, or MRI) of adequate quality available for comparison, the presence of foci of [^{18}F]FDG uptake are classified as BMI [34].

4. Bone marrow involvement – tumour type specific considerations

4.1. Haemato-oncology

*4.1.1. **Leukemia***

Acute Lymphoblastic Leukaemia (ALL) is the most common subtype of paediatric leukaemia, compromising 80 % of all cases. Acute leukaemia classically presents with diffuse involvement of the bone marrow that shows as low T1 and high T2 signal intensity with marked diffusion restriction at MRI. Detection of these often homogeneous and symmetrical abnormalities requires knowledge of normal signal intensity of bone marrow for age and may otherwise easily lead to erroneous interpretation [1]. MRI has a limited role in diagnosis, response evaluation and surveillance of leukaemia, where complete blood counts, bone marrow aspirates/biopsies and cerebral liquor investigations are diagnostic cornerstones. However, in children, leukaemia can present with non-specific symptoms like back-pain, painful extremities, and limping, and MRI to look for musculoskeletal pathology may be performed. It is then extremely important to be aware of bone marrow infiltration, which can easily be overlooked, particularly in diffuse symmetrical involvement [15]. Furthermore, leukaemia relapse can sometimes be detected by MRI before the recurrence is established with bone marrow aspirates because of sampling bias of the latter. Relapse can be differentiated from regenerating bone marrow by detecting mass effect, cortical bone destruction and an associated extraosseous extension of disease. Myeloid Sarcoma is an extramedullary tumour of immature granulocytic cells, often found either concurrently or following a previously diagnosed AML [35].

[^{18}F]FDG-PET/CT is not routinely used in the assessment of leukaemia but (diffuse or focally) increased uptake of [^{18}F]FDG can be a

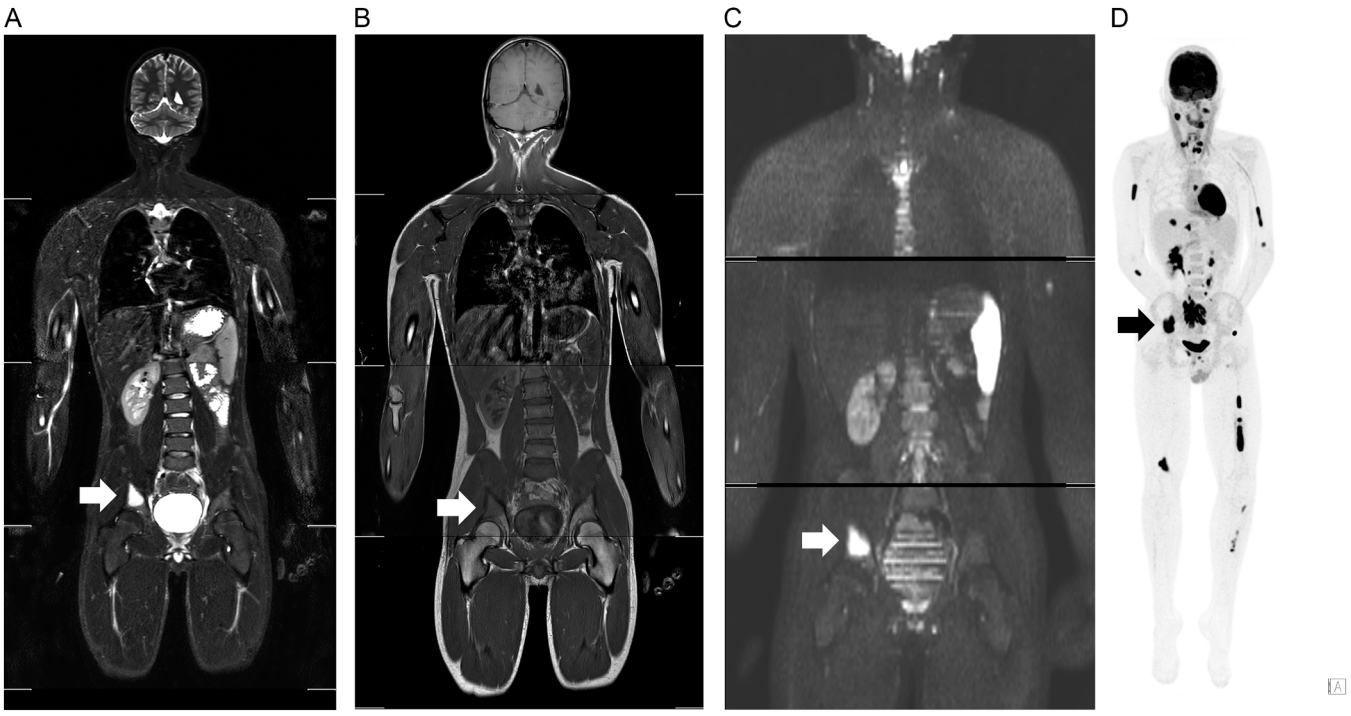

Fig. 4. Coronal whole-body STIR (A), T1w (B), and maximum intensity projection grayscale diffusion weighted (C) MRI images in a boy, 16 years of age, with a mature B-cell NHL, illustrating focal BMI in the right iliac wing (arrow in A-C) with high signal intensity on STIR (A), intermediate-low signal intensity on T1 (B), and signs of diffusion restriction on DWI (C). Coronal whole -body [^{18}F]FDG-PET image (D) for correlation illustrating the increased focal [^{18}F]FDG-uptake of the bone marrow lesion in the right iliac wing (arrow). In addition, several other focal bone marrow lesions with increased [^{18}F]FDG-uptake can be seen throughout the skeleton consistent with multifocal BMI (also visible on the whole-body MRI, not shown).

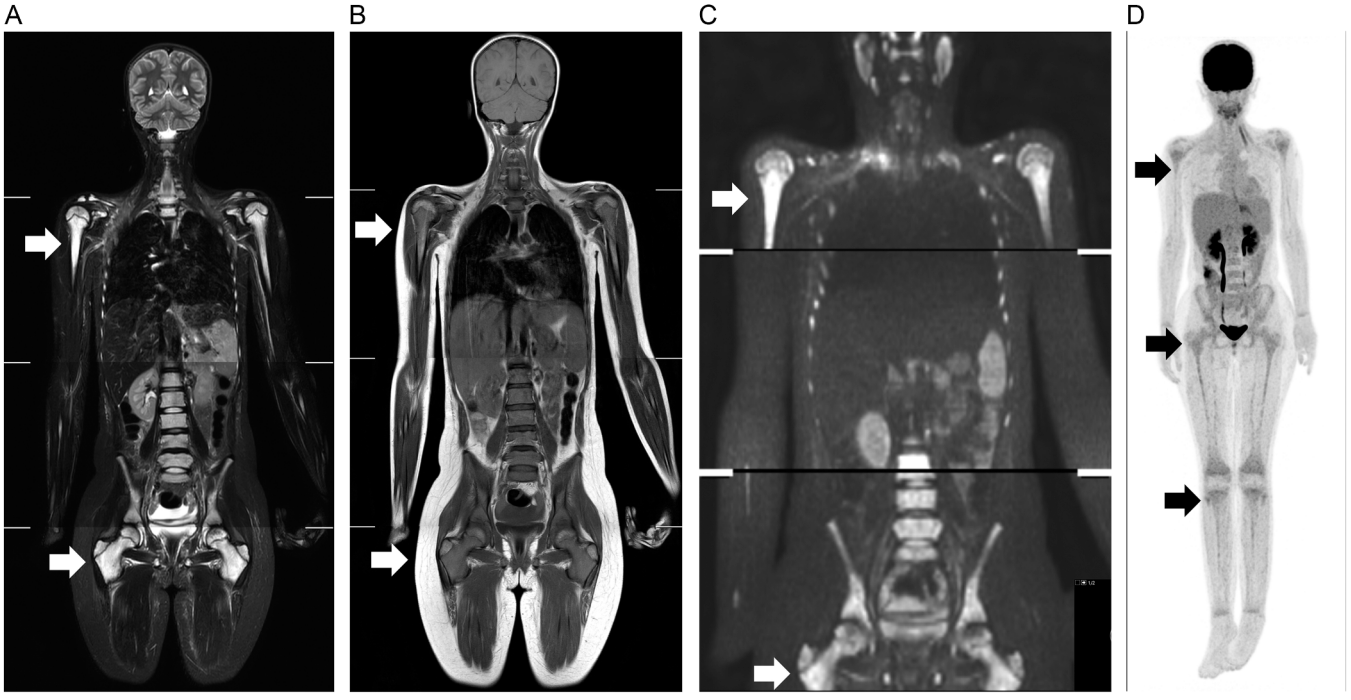

Fig. 5. Coronal whole-body STIR (A), T1w (B), and maximum intensity projection grayscale diffusion weighted (C) MRI images in a girl, 13 years of age, with an intra-abdominal Burkitt lymphoma, illustrating diffuse BMI (arrows in A-C) with high signal intensity on STIR (A), intermediate-low signal intensity on T1 (B), and signs of diffusion restriction on DWI (C). Coronal whole-body [^{18}F]FDG-PET image (D) for correlation, illustrating the diffuse [^{18}F]FDG-uptake of the bone marrow throughout the skeleton (arrows), in this case comparable with the [^{18}F]FDG-uptake in the liver parenchyma due to corticosteroid therapy that was already started some days before the PET scan.

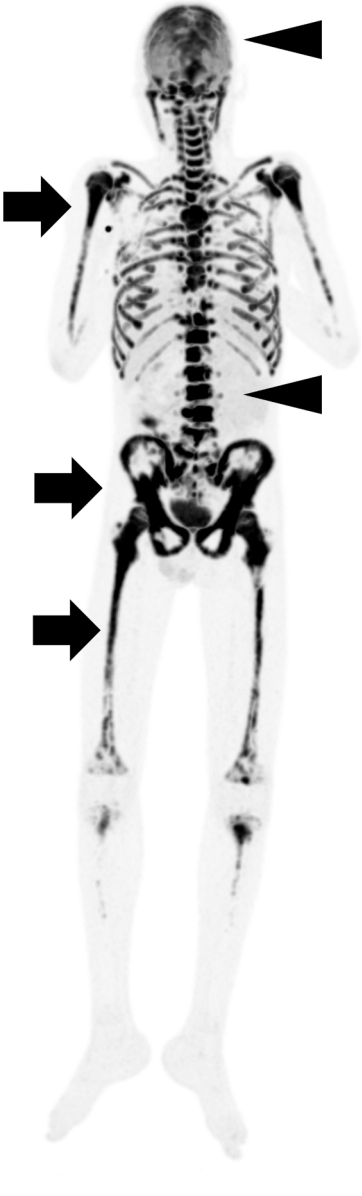

Fig. 6. Pre-treatment coronal whole-body [^{18}F]FDG-PET image in a boy, 13 years of age, with post-transplant lymphoproliferative disease (PTLD) after renal transplantation, illustrating pathological diffuse [^{18}F]FDG-uptake of the bone marrow throughout the skeleton (arrows and arrowheads), higher than the [^{18}F]FDG-uptake in the liver, indicating diffuse BMI.

characteristic finding in leukaemia patients. It can be helpful in the evaluation of extramedullary infiltration, monitoring of leukaemia relapse, detection of Richter's transformation and assessment of the inflammatory activity associated with acute graft versus host disease [36]. When interpreting [^{18}F]FDG-PET/CT, knowledge of the [^{18}F]FDG uptake patterns in patients with leukaemia is important, as these patients can present with fever of unknown origin.

4.1.2. *Lymphoma*

Figs. (4–6) The detection of BMI is important for accurate staging because the presence of BMI indicates the highest stage of disease in both Hodgkin lymphoma (HL) and non-Hodgkin lymphoma (NHL) [37].

BMI in paediatric HL is seen in around 14 % of cases [38]. [^{18}F]FDG-PET/CT and whole-body MRI (WB-MRI) can detect BMI with high accuracy. The major limitation of bone marrow biopsies is related to sampling error in focal bone marrow disease, that is often seen in HL. A systematic review has reported [^{18}F]FDG-PET/CT to be highly accurate for bone marrow infiltration in both HL and NHL, with pooled sensitivity and specificity of 97 % and 99 %, respectively [39]. Therefore, bone marrow biopsies can often be omitted and the current guidelines already recommend [^{18}F]FDG-PET/CT only for assessing BMI in paediatric HL [37,40].

As HL occurs in the older paediatric age group, WB-MRI is a sensitive imaging technique for detecting BMI, because of the normal, physiologic fatty conversion of bone marrow in these children and adolescents that provides excellent contrast with the signal intensities of BMI [1]. Diffuse BMI, although not often detected in paediatric lymphomas, should, however, be differentiated from reactive bone marrow changes generally seen at first presentation of lymphomas. This reactive bone marrow will show moderate diffuse FDG uptake at [^{18}F]FDG-PET/CT of the axial skeleton.

Response assessment of BMI during treatment is preferably performed with [^{18}F]FDG-PET/CT, because the signal aberrations at conventional MRI persist for a longer period than the malignant cells are detected [41]. The role of DWI with ADC measurements remains uncertain and in case of small residual lesions, the reliability of ADC measurements in these lesions is questionable.

In childhood NHL, the International Pediatric NHL staging system (IPNHLSS) is used, related to the predominant extra-nodal involvement. This staging system restricts stage IV for bone marrow and CNS involvement. BMI is still diagnosed with bone marrow biopsies in NHL and the role of [^{18}F]FDG-PET/CT and/or WB-MRI is not yet clarified [42], probably due to the large variability of subtypes and their varying aggressiveness. However, the recently published Children's Oncology Group (COG) imaging recommendations in paediatric lymphoma encourage the use of [^{18}F]FDG-PET/CT for staging of most NHL subtypes and for interim and end of therapy response assessments [43].

Primary involvement of the bone is a rare manifestation of NHL in children and adolescents [41]. It is characterised by a non-specific and indolent clinical presentation. On MRI, epiphyseal involvement of the lower extremity with infarct-like appearance is described.

4.1.3. *Histiocytic diseases*

Histiocytic disorders of childhood are characterized by the accumulation of cells with a macrophage or dendritic phenotype in various tissues. It represents a wide spectrum of conditions. Langerhans cell histiocytosis (LCH) is the most common histiocytic disorder in children and young adults [30,44]. It can manifest at any age with a broad spectrum of clinical behaviour ranging from self-limiting disease to a multi-system life-threatening condition. Any organ can potentially be affected. The current guideline recommends a radiographic skeletal survey for assessing bone involvement [44]. Whole-body MRI (WB-MRI) is a radiation free alternative with a high sensitivity. A few studies have compared the diagnostic accuracy of WB-MRI compared to the radiographic skeletal survey and/or bone scintigraphy, that show a higher sensitivity of WB-MRI for skeletal and extra-skeletal lesions [45–47]. However, the clinical implications with the risk of upstaging and subsequent overtreating remain uncertain. A typical manifestation of LCH in bone is the vertebra plana of the spine. The imaging features of LCH in bone at MRI are characterized by remarkable surrounding oedema with varying degree of diffusion restriction and can therefore overlap with infection and malignancy [30].

Studies suggest that [^{18}F]FDG-PET/CT has a complementary role for the staging of LCH [48]. It could be considered helpful due to its ability to determine metabolically active disease [49], although it is not currently recommended by clinical guidelines.

4.2. *Metastatic disease*

4.2.1. *Neuroblastoma*

Around 50 % of patients diagnosed with neuroblastoma presents with metastatic disease, often to the bone marrow [50]. In case of

widespread bone marrow disease, children present with bone pain, limping, irritability and being general ill. Not rarely, these children are initially misdiagnosed with osteomyelitis. In infants and young children, diffuse bone marrow metastases can be difficult to detect with MRI due to the abundant, predominant red bone marrow characteristics in this population. Oedema or extra-osseous extension could serve as tell-tale. In heavily involved bone marrow, imaging features suggestive for osteonecrosis can be seen already at presentation (Fig. 7).

Nuclear medicine studies are the diagnostic cornerstone for diagnosis and response assessment in neuroblastoma. In current protocols, [^{123}I]mIBG scintigraphy is the standard nuclear medicine examination [51]. Approximately 90 % of neuroblastoma cases show an affinity for [^{123}I]mIBG scintigraphy [52]. The [^{123}I]mIBG scan comprises of a planar whole-body scintigram 24 hours after tracer injection that is followed by an additional single photon emission computed tomography (SPECT)/CT, typically of the thorax and abdomen (Fig. 8). In [^{123}I]mIBG negative disease, [^{18}F]FDG-PET/CT is generally advised. However, an important disadvantage of the use of [^{18}F]FDG-PET/CT is the treatment related reactive bone marrow changes that shows relatively high [^{18}F]FDG uptake, hampering evaluation of skeletal or bone marrow lesions in follow-up scans. More specific tracers (e.g. somatostatin receptor targeted tracers like ([^{68}Ga]DOTATOC) or dopamine synthesis targeted tracers like [^{18}F]DOPA) will most likely result in more accurate assessment of disease at presentation and during follow-up [53]. Furthermore, a more recent development is the PET-tracer ^{18}F-meta-fluorobenzylguanidine ([^{18}F]mFBG), a molecule labelled with ^{18}F that is almost the same as the SPECT-tracer [^{123}I]mIBG. It shows great promise as future diagnostic tool for diagnosis and response assessment in neuroblastoma [54,55].

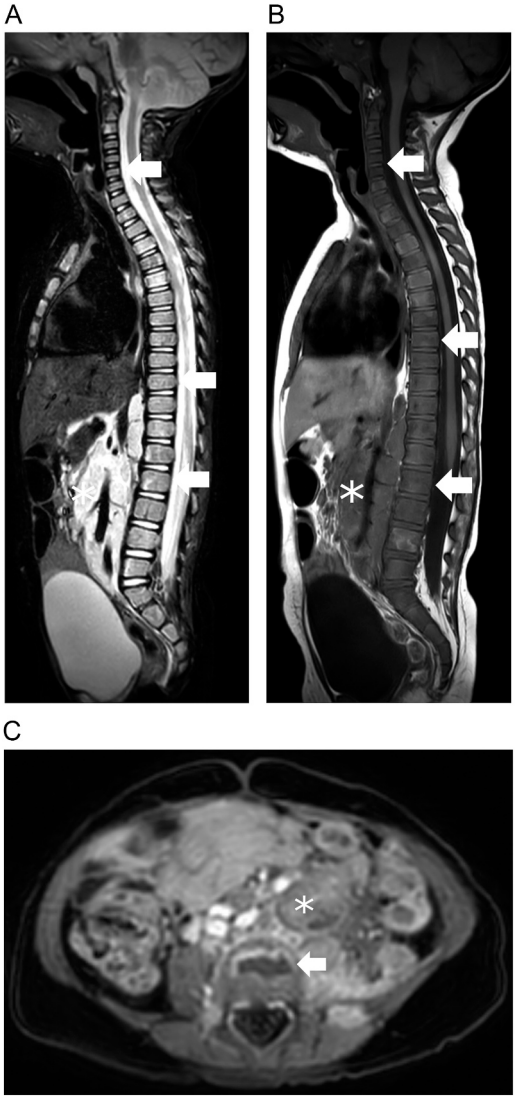

Fig. 7. Sagittal STIR (A), and T1w (B) MRI images in a boy, 1 year of age, with neuroblastoma illustrating extensive multifocal BMI of the whole spine (arrows in A & B) with inhomogeneous high signal intensity on STIR (A), and intermediate-low signal intensity on T1 (B) of all vertebrae. The asterisk marks the retroperitoneal located neuroblastoma. The axial contrast enhanced T1w (C) MRI image at the level of L4 illustrates the osteonecrotic transformation of the bone marrow metastasis (arrow).

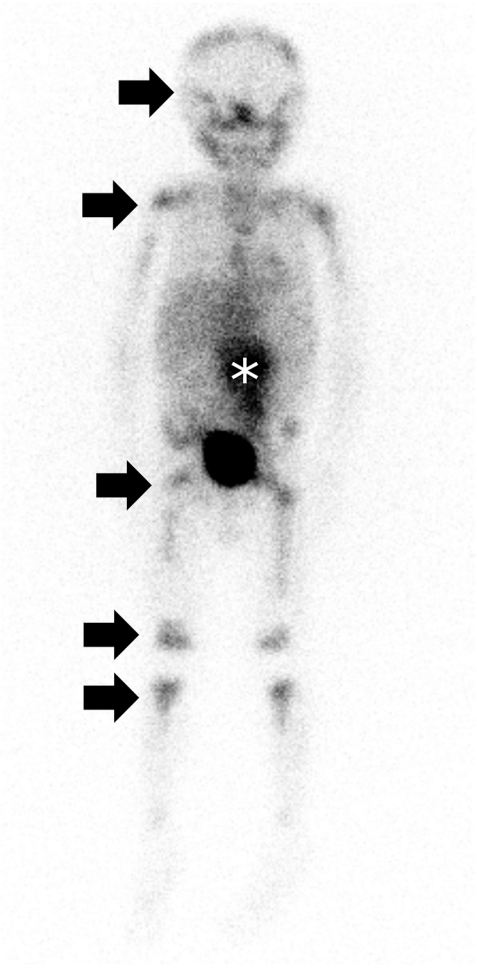

Fig. 8. Coronal whole-body [^{123}I]mIBG image in the same patient as Fig. 7, illustrating the multifocal increased [^{123}I]mIBG-uptake of the bone marrow throughout the skeleton (arrows) indicating multifocal bone marrow metastases. The asterisk marks the [^{123}I]mIBG-uptake in the retroperitoneal located neuroblastoma.

Within the current treatment protocols of the Society of Paediatric Oncology Europe Neuroblastoma (SIOPEN) and Children's Oncology Group (COG), response assessment of BMI during treatment is performed by nuclear medicine techniques such as [^{123}I]mIBG scintigraphy, either through the SIOPEN or Curie score [56–58]. These semi-quantitative scores evaluate skeletal metastasis uptake on a score of 0–6 in 12 anatomical regions (SIOPEN), or 9 regions ranging from 0 to 3 with a tenth region for soft tissue (Curie). Although initially mainly used in clinical trials and comparative imaging studies, these standardized methods for quantifying disease burden are nowadays also used in daily practice for staging disease, evaluating treatment response, and assessing prognosis.

The role of MRI in response assessment of BMI is uncertain because

the signal aberrations at conventional MRI persist for a longer time than the malignant cells can be detected. The use of DWI with ADC measurements has not yet been proven. However, due to the strong diffusion restriction of poorly differentiated neuroblastoma, in daily clinical practice, MRI with DWI is considered to serve as a sensitive technique for detection of progressive or recurrent disease.

4.2.2. *Rhabdomyosarcoma*

Rhabdomyosarcoma (RMS) is a rare soft tissue sarcoma occurring predominantly in children and adolescents. It is highly aggressive and can arise anywhere in the human body. This most common paediatric soft tissue sarcoma affects around 400 new patients ages 0–19 years each year across Europe. Imaging should assess nodal involvement and distant metastases which are primarily found in the lungs, and bone marrow, although it can metastasise to any site in the body [59]. RMS with bone marrow metastases accounts for approximately 6–16 % of all RMS cases as part of widespread disease [60]. Its most aggressive subtypes (alveolar RMS, FOXO1 fusion status) may initially present like a hematologic malignancy with diffuse bone marrow involvement in absence of a significant soft tissue tumour [61]. In these cases, whole body imaging by WB-MRI or [^{18}F]FDG-PET/CT (or PET/MRI) may provide the first clue to the diagnosis as it can depict the abnormal signal intensity and heterogenous enhancement of the bone marrow as well as the clinically silent primary tumour in the distal parts of a limb [62]. The prognosis of these patients is poor with a high risk of recurrence [60]. [^{18}F]FDG-PET/CT should always be performed from head to toe (and include chest CT) in order to evaluate the entire bone marrow, regional lymph nodes, lungs, and other sites of involvements. It has higher sensitivity in detecting distant metastases including BMI than standard radiology work-up with MRI, chest CT and bone scintigraphy [63].

4.2.3. *Bone tumors*

Although rare in absolute numbers, osteosarcoma (OS) and Ewing's sarcoma (ES) are the most frequent primary bone tumours in children and adolescents [64]. It is well known that the intramedullary tumour extension may considerably exceed that of the soft tissue tumour and the osteolysis visible on conventional radiographs. As primary complete resection is an important prognostic factor, delineating the exact tumour margins is crucial for preoperative planning. MRI is the modality of choice to depict the entire tumour and its relation to adjacent structures. The border between tumour and normal bone marrow is best delineated on a T1w sequence without fat suppression as on T2w fat suppressed images the margin may be obscured by the peritumoral oedema (Fig. 9) [65]. However, an additional safety margin of 10 mm is recommended [66]. Diffusion weighted MRI, and [^{18}F]FDG-PET/CT contribute to additional (functional) information but not in the delineation of the primary tumour due to less spatial accuracy (Fig. 10). In the primary tumour, [^{18}F]FDG-PET/CT adds information about the area of the highest metabolism (SUV_{max}) for biopsy guidance. Furthermore, early (5 week) changes in SUV_{max} has shown to be predictive of a histologic response in patients with OS [67], and after induction chemotherapy in patients with ES [68]. Diagnostic accuracy may be further improved by combining [^{18}F]FDG-PET/CT with DWI MRI [69].

OS and ES may metastasize to the lymph nodes, bone marrow, and lungs. [^{18}F]FDG-PET/CT has proven to be highly useful for the initial staging of both types of bone tumours including identifying distant lymph node and bone marrow metastases [70,71]. Skip lesions may be found (by MRI and/or [^{18}F]FDG-PET/CT) in the same bone or on the opposite side of the adjacent joint. They occur in 6,5 % of cases [72] and influence the surgical approach as well as the overall prognosis [73]. In addition, ES may rarely cause BMI which cannot be detected by WB-MRI and/or [^{18}F]FDG-PET/CT. Some authors, therefore, conclude that there is no additional value in performing a bone marrow biopsy in patients who undergo [^{18}F]FDG-PET/CT or WB-MRI as it does not alter the standard of care management [74]. This is still a matter of debate as others report cases of BMI without findings on [^{18}F]FDG-PET/CT or WB-MRI [75]. Consensus recommendations, however, consider it reasonable to omit bone marrow aspirate or biopsy in case of a negative [^{18}F]FDG-PET/CT [76].

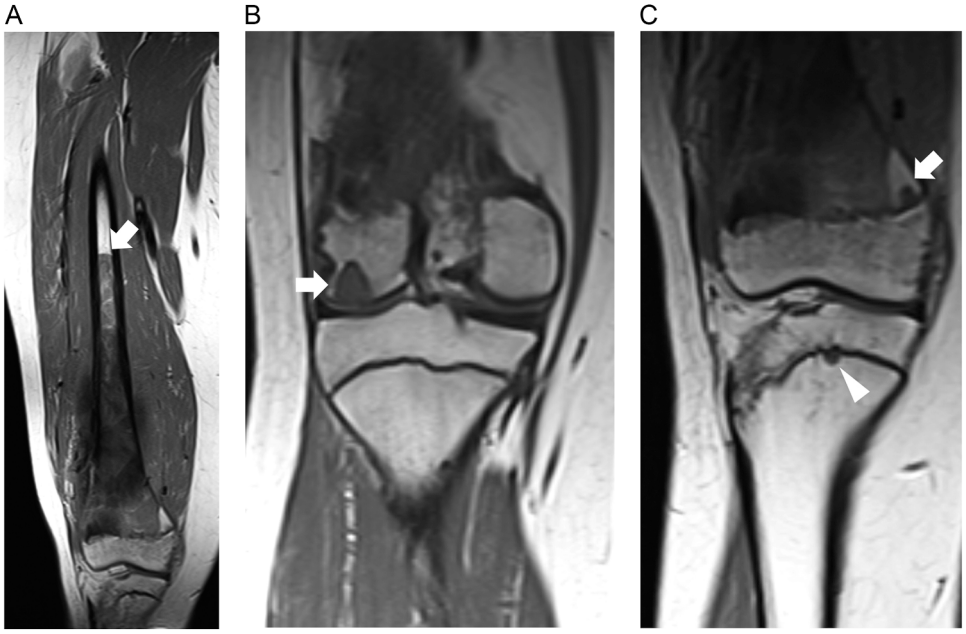

Fig. 9. Coronal T1w MRI images of the right femur (A), and right knee (B & C), in a boy, 15 years of age, with an osteosarcoma, illustrating the distinct border between the intraosseous tumour and the fatty bone marrow (arrow in A). In addition, there are skip lesions in the distal epiphysis (arrow in B), and metaphysis (arrow in C) of the same femur. Even more relevant for resection planning is the skip lesion in the proximal metaphysis of the right tibia (arrowhead in C) which was less conspicuous on DWI and [^{18}F]FDG-PET because of the adjacent physis (not shown).

Fig. 10. Coronal whole-body [^{18}F]FDG-PET image in a boy, 13 years of age, with a Ewing sarcoma, illustrating increased multifocal [^{18}F]FDG-uptake throughout the skeleton, in particular in the spinal column, pelvis, and proximal and distal femora (arrowheads), indicating multifocal bone marrow metastases. The increased [^{18}F]FDG-uptake in the primary tumour at the level of the left iliac wing is indicated by the arrow.

5. Treatment related bone marrow changes

5.1. MRI

The accurate evaluation of treatment response in BMI is difficult on MRI, related to the persistent signal changes that can be seen for a long time, also after treatment. These signal changes do not necessarily correlate to disease activity. The role of DWI and contrast-enhancement to evaluate treatment response of known bone marrow lesions remain uncertain [22]. In a study in children with primary bone lymphoma, all patients had bone marrow changes on long-term follow up which could be due to the disease itself but also to direct treatment-related changes [41]. Osteonecrosis of the bone marrow is frequently seen in lymphoproliferative disorders, both due to ischemia caused by marrow infiltration but also as a result of treatment as such, as both chemotherapy and steroids increase the risk of osteonecrosis [77,78].

Radiotherapy will influence the bone marrow included in the radiation-field. The induced changes and the ability of the bone marrow to recover from this depends on the age of the child and the radiation dose. Initially the marrow will develop oedema and sometimes haemorrhage. After 3–6 weeks there is a depletion of red marrow after which fat replacement will gradually occur. End stage fat replacement typically shows sharp demarcation on T1w TSE images (Fig. 11). Red marrow regeneration occurs in areas where recovery is possible. All these processes influence signal and can in part show very heterogenous MRI-patterns [1,79].

Low T2 signal due to bone marrow depletion during therapy or signal loss due to iron deposition may occur depending on treatment and the number of blood transfusions received. The opposite, increased T2 signal due to increased cellularity, e.g. following successful bone marrow transplantation, from marrow reconversion, as a response to stress, or administration of granulocyte colony-stimulating factors (G-CSF) during therapy, may also be seen. Signs of increased cellularity in the bone marrow can be difficult to differentiate from disease relapse on imaging alone. Close clinical-radiological correlation is pivotal in the interpretation of treatment related bone marrow changes.

5.2. [^{18}F]FDG-PET

Increased diffuse homogenous bone marrow uptake of [^{18}F]FDG is a well-described response to cancer therapy and includes physiologic

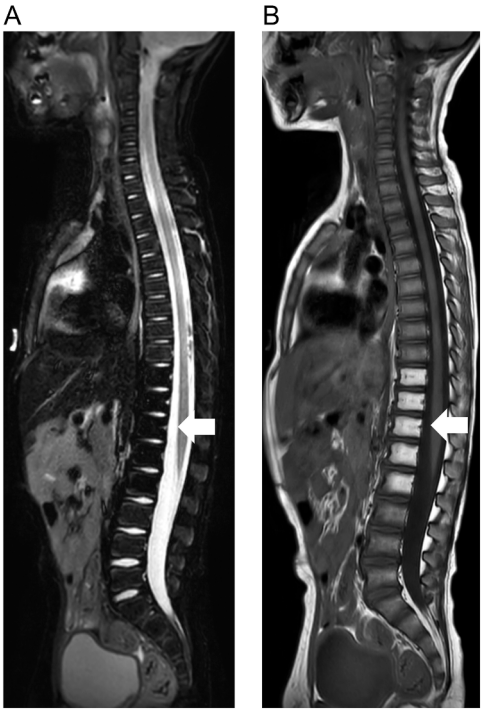

Fig. 11. Sagittal STIR (A), and T1w (B) MRI images in a boy, 4 years of age, with a neuroblastoma for which he was treated with chemotherapy, surgery, and radiotherapy. Follow-up 4 months after end of radiotherapy shows complete fatty replacement of the bone marrow of the lower thoracic and upper lumbar vertebrae with a sharp demarcation and pronounced low signal intensity on STIR (arrow in A), and high signal intensity on T1 (arrow in B).

rebound after chemotherapy which usually resolves within a month. Pharmacologic hematopoietic stimulation with G-CSF to hasten marrow recovery, shows a diffuse intense [^{18}F]FDG uptake. An interval of 3 weeks between administration of the long-acting form of G-CSF and [^{18}F]FDG-PET/CT is suggested to minimize the increased marrow uptake caused by G-CSF [80]. If [^{18}F]FDG-PET/CT is done in the middle of chemotherapy (interim PET) and the study cannot be postponed, the reduced sensitivity of bone marrow evaluation due to the G-CSF effect should be explained in the report.

After treatment of marrow infiltrating disease, follow-up [^{18}F]FDG-PET/CT may show regions of minimal [^{18}F]FDG uptake at sites of former bone marrow disease. In the same way, minimal marrow uptake may be seen within the field of radiotherapy. Reduced bone marrow [^{18}F]FDG uptake can be seen several months after radiotherapy and is due to the replacement of bone marrow by fatty tissue.

Increased focal [^{18}F]FDG uptake in bone marrow rarely reflects treatment-related marrow stimulation and usually represents BMI by disease. Focal increased and inhomogeneous [^{18}F]FDG uptake in the bone marrow and/or corresponding to an anatomical lesion on CT is in keeping with malignant BMI.

6. Conclusions

Multimodality bone marrow imaging plays an essential role in paediatric oncology and typically involve MRI and/or nuclear medicine techniques such as [^{18}F]FDG-PET/CT. These imaging modalities provide complementary information about BMI in paediatric cancers, helping in diagnoses, staging, treatment planning, and monitoring of response to therapy. Knowledge of normal age-related physiological, as well as disease and therapy related bone marrow changes is crucial for a correct imaging interpretation and often includes a solid clinico-radiological correlation, preferably in a multidisciplinary setting.

Funding

None.

CRediT authorship contribution statement

Rutger A.J. Nievelstein: Writing – review & editing, Writing – original draft, Visualization, Supervision, Conceptualization. **Lise Borgwardt:** Writing – review & editing, Writing – original draft. **Thekla Von Kalle:** Writing – review & editing, Writing – original draft. **Annemieke S. Littooij:** Writing – review & editing, Writing – original draft. **Lil-Sofie Ording Müller:** Writing – review & editing, Writing – original draft. **Nelleke Tolboom:** Writing – review & editing, Writing – original draft.

Declaration of Competing Interest

All authors have declared no conflicts of interest.

References

[1] B.Y. Chan, K.G. Gill, S.L. Rebsamen, J.C. Nguyen, MR imaging of pediatric bone marrow, Radiographics 36 (2016) 1911–1930, https://doi.org/10.1148/rg.2016160056.
[2] R.A.J. Nievelstein, A.S. Littooij, Whole-body MRI in paediatric oncology, Radio. Med 121 (2016) 442–453, https://doi.org/10.1007/s11547-015-0600-7.
[3] M.D. Patel, J. Brain, N.A. Chauvin, Pearls and pitfalls in imaging bone marrow in pediatric patients, Semin Ultrasound CT MRI 41 (2020) 472–487, https://doi.org/10.1053/j.sult.2020.05.012.
[4] M.G. Chiarilli, A. Delli Pizzi, D. Mastrodicasa, M.P. Febo, B. Cardinelli, B. Consorte, A. Cifaratti, V. Panara, M. Caulo, G. Cannataro, Bone marrow magnetic resonance imaging: physiologic and pathologic findings that radiologist should know, La Radiol. Med. 126 (2021) 264–276, https://doi.org/10.1007/s11547-020-01239-2.
[5] M.P.A. Gómez, C.A. Benanvent, P. Simoni, P.M. Aguiar, A. Bazzocchi, F. Aparisi, Imaging of bone marrow: from science to practice, Semin Musculoskelet. Radio. 26 (2022) 396–411, https://doi.org/10.1055/s-0042-1745803.
[6] C. Mourad, A. Cosentino, M.N. Lalonde, P. Omoumi, Advances in bone marrow imaging: strengths and limitations from a clinical perspective, Semin Musculoskelet. Radio. 27 (2023) 3–21, https://doi.org/10.1055/s-0043-1761612.
[7] Y. Maeder, V. Dunet, R. Richard, F. Becce, P. Omoumi, Bone marrow metastases: T2- weighted Dixon Spin-Echo Fat Images Can Replace T1-weighted Spin-Echo? Radiology 286 (2018) 948–959.
[8] L. Tanturi de Horatio, P.K. Zadig, E. Von Brandis, L.S. Ording Müller, K. Rosendahl, D.F.M. Avenarius, Whole-body MRI in children and adolescents: Can T2-weighted Dixon fat-only images replace standard T1-weighted images in the assessment of bone marrow? EJR 166 (2023) 110968 https://doi.org/10.1016/j.ejrad.2023.110968.
[9] T. Kirchgesner, S. Acid, V. Perlepe, F. Lecouvet, B. Vande Berg, Two-point Dixon fat-water swapping artifact: lesion mimicker at musculoskeletal T2-weighted MRI, Skelet. Radio. 49 (12) (2020) 2081–2086, https://doi.org/10.1007/s00256-020-03512-x.
[10] A. Chaturvedi, Pediatric skeletal diffusion-weighted magnetic resonance imaging: part 1 — technical considerations and optimization strategies, Pedia Radio. 51 (2021) 1562–1574.
[11] A. Chaturvedi, Pediatric skeletal diffusion-weighted magnetic resonance imaging, part 2: current and emerging applications, Pedia Radio. 51 (2021) 1575–1588.
[12] L.S. Ording Müller, D. Avenarius, O.E. Olsen, High signal in bone marrow at diffusion-weighted imaging with body background suppression (DWIBS) in healthy children, Pedia Radio. 41 (2) (2011 Feb) 221–226, https://doi.org/10.1007/s00247-010-1774-8.
[13] P. Raijah, A. Parakh, F. Kay, D. Baruah, A.R. Kambadakone, S. Leng, Update on multienergy CT: physics, principles, and applications, RadioGraphics 40 (2020) 1284–1308, https://doi.org/10.1148/rg.2020200038.
[14] A. Agool, A.W.J.M. Glaudemans, H.H. Boersma, R.A.J.O. Dierkckx, E. Vellenga, R. H.J.A. Slart, Radionuclide imaging of bone marrow disorders, Eur. J. Nucl. Med Mol. Imaging 38 (2011) 166–178.
[15] R.P. Guillerman, Marrow: red, yellow and bad, Pedia Radio. 43 (Suppl 1) (2013) S181–S192, https://doi.org/10.1007/s00247-012-2582-0.
[16] R.A.J. Nievelstein, A.S. Littooij, Chapter 7: Whole body MRI in pediatric oncology, in: S.D. Voss, K. McHugh (Eds.), Imaging in pediatric oncology, Springer Nature, 2019.
[17] N. Shabshin, M.E. Schweitzer, W.B. Morrison, J.A. Carrino, M.S. Keller, L. E. Grissom, High-signal T2 changes of the bone marrow of the foot and ankle in children: red marrow or traumatic changes?, in: Pediatr Radiol, 36, 2006, pp. 670–676, https://doi.org/10.1007/s00247-006-0129-y.
[18] L.O. Ording Müller, D. Avenarius, B. Damasio, O.P. Eldevik, C. Malattia, K. Lambot-Juhan, L. Tanturri, C.M. Owens, K. Rosendahl, The paediatric wrist revisited: redefining MR findings in healthy children, Ann. Rheum. Dis. 70 (2011) 605–610.
[19] E. Von Brandis, P.K. Zadig, D.F.M. Avenarius, B. Flatø, P.K. Knudsen, V. Lilleby, B. Nguyen, K. Rosendahl, L.S. Ording Müller, Whole body magnetic resonance imaging in healthy children and adolescents. Bone marrow appearances of the axial skeleton, Eur. J. Radio. 154 (2022) 110425, https://doi.org/10.1016/j.ejrad.2022.110425.
[20] P.K. Zadig, E. Von Brandis, B. Flatø, L.S. Ording Müller, E.B. Nordal, Tanturri de Horatio, L. Rosendahl, K. Avenarius, DFM. Whole body magnetic resonance imaging in healthy children and adolescents: bone marrow appearances of the appendicular skeleton, Eur. J. Radio. 153 (2022) 110365, https://doi.org/10.1016/j.ejrad.2022.110365.
[21] A. Rashidi, L. Baratto, P. Jayapal, A.J. Theruvath, E.B. Greene, R. Lu, S.L. Spunt, H. E. Daldrup-Link, Detection of bone marrow metastases in children and young adults with solid cancers with diffusion-weighted MRI, Skelet. Radio. 52 (2023) 1179–1192, https://doi.org/10.1007/s00256-022-04240-0.
[22] M. Winfeld, S. Ahlawat, N. Safdar, Utilization of chemical shift MRI in the diagnosis of disorders affecting pediatric bone marrow, Skelet. Radio. 45 (2016) 1205–1212, https://doi.org/10.1007/s00256-016-2403-x.
[23] A. Shammas, R. Lim, M. Charron, Pediatric FDG PET/CT: physiologic uptake, normal variants, and benign conditions, RadioGraphics 29 (2009) 1467–1486, https://doi.org/10.1148/rg.295085247.
[24] U. Nygaard, L.V. Larsen, N.H. Vissing, M.L. von Linstow, C. Myrup, A.K. Berthelsen, A. Poulsen, L. Borgwardt, Unexplained fever in children-Benefits and challenges of FDG-PET/CT, Acta Paediatr. 111 (11) (2022 Nov) 2203–2209, https://doi.org/10.1111/apa.16503. Epub 2022 Aug 13. PMID: 36210785.
[25] G.P. Schmidt, S.O. Schoenberg, M.F. Reiser, A. Baur-Melnyk, Whole-body MR imaging of bone marrow, Eur. J. Radio. 55 (1) (2005) 33–40.
[26] S.P. Ryan, E. Weinberger, K.S. White, D.W.W. Shaw, K. Patterson, V. Nazar-Stewart, J. Miser, MR imaging of bone marrow in children with osteosarcoma: effect of granulocyte colony-stimulating factor, AJR 165 (1995) 915–920.
[27] K.L. Atkin, M.R. Ditchfield, The role of whole-body MRI in pediatric oncology, J. Pedia Hematol. Oncol. 36 (2014) 342–352.
[28] K.W. Carroll, J.F. Feller, P.F. Tirman, Useful internal standards for distinguishing infiltrative marrow pathology from hematopoietic marrow at MRI, J. Magn. Reson Imaging 7 (2) (1997) 394–398, https://doi.org/10.1002/jmri.1880070224.
[29] D.C. Zajick, W.B. Morrison, M.E. Schweitzer, J.A. Parellada, J.A. Carrino, Benign and malignant processes: normal values and differentiation with chemical shift MR imaging in vertebral marrow, Radiology 237 (2005) 590–596.
[30] J.D. Samet, J. Deng, K. Schafernak, N.C. Arva, X. Lin, J. Peevey, L.M. Fayad, Quantitative magnetic resonance imaging for determining bone marrow fat fraction at 1.5 T and 3.0 T: a technique to noninvasively assess cellularity and potential malignancy of the bone marrow, Pedia Radio. 51 (2021) 94–102.
[31] M.E. Schweitzer, C. Levine, D.G. Mitchell, F.H. Gannon, L.G. Gomella, Bull's-eyes and halos: useful MR discriminators of osseous metastases, Radiology 188 (1) (1993) 249–252.

[32] H. Jadvar, L.P. Connolly, F.H. Fahey, B.L. Shulkin, PET and PET/CT in pediatric oncology, Semin Nucl. Med 37 (5) (2007) 316–331.

[33] Y. Sugawara, S.J. Fisher, K.R. Zasadny, P.V. Kison, L.H. Baker, R.L. Wahl, Preclinical and clinical studies of bone marrow uptake of fluorine-1-fluorodeoxyglucose with or without granulocyte colony-stimulating factor during chemotherapy, J. Clin. Oncol. 16 (1) (1998) 173–180, https://doi.org/10.1200/JCO.1998.16.1.173.

[34] D. Kaddu-Mulindwa, B. Altmann, G. Held, S. Angel, S. Stilgenbauer, L. Thurner, M. Bewarder, M. Schwier, M. Pfreundschuh, M. Löffler, K. Menhart, J. Grosse, M. Ziepert, K. Herrmann, U. Dührsen, A. Hüttmann, F. Barbato, V. Poeschel, D. Hellwig, FDG PET/CT to detect bone marrow involvement in the initial staging of patients with aggressive non-Hodgkin lymphoma: results from the prospective, multicenter PETAL and OPTIMAL>60 trials (Oct), Eur. J. Nucl. Med Mol. Imaging 48 (11) (2021) 3550–3559, https://doi.org/10.1007/s00259-021-05348-6.

[35] M.F. Tannenbaum, S. Noda, S. Cohen, J.G. Rissmiller, A.M. Golja, D.M. Schwartz, Manifestations of pediatric hematologic malignancies, Am. J. Roentgenol. 214 (2) (2020 Feb) 455–464, https://doi.org/10.2214/AJR.19.21833.

[36] Z. Zhao, Y. Hu, J. Li, Y. Zhou, B. Zhang, S. Deng, Applications of PET in diagnosis and prognosis of leukemia, Technol. Cancer Res Treat. 19 (2020) 1–12.

[37] B.D. Cheson, R.I. Fisher, S.F. Barrington, F. Cavalli, L.H. Schwartz, E. Zucca, T. A. Lister, Recommendations for initial evaluation, staging, and response assessment of Hodgkin and non-Hodgkin lymphoma: the Lugano classification, J. Clin. Oncol. 32 (2014) 3059–3067, https://doi.org/10.1200/JCO.2013.54.8800.

[38] A. Englund, I. Glimelius, K. Rostgaard, K.E. Smedby, S. Eloranta, D. Molin, T. Kuusk, de Nully Brown, P. Kamper, P. Hjalgrim, H. Ljungman, G. Hjalgrom, LL. Hodgkin lymphoma in children, adolescents and young adults – a comparative study of clinical presentation and treatment outcome, Acta Oncol. 57 (2018) 276–282.

[39] Z. Li, C. Li, B. Chen, L. Shi, F. Gao, P. Wang, W. Sun, FDG-PET/CT versus bone marrow biopsy in bone marrow involvement in newly diagnosed paediatric lymphoma: a systematic review and meta-analysis, J. Orthop. Surg. Res 16 (2021) 482.

[40] S. Purz, C. Mauz-Körholz, D. Körholz, D. Hasenclever, A. Krausse, I. Sorge, K. Ruschke, M. Stiefel, H. Amthauer, O. Schober, W.T. Kranert, W.A. Weber, U. Haberkorn, P. Hundsdörfer, K. Ehlert, M. Becker, J. Rössler, A.E. Kulozik, O. Sabri, R. Kluge, 18F]Fluorodeoxyglucose positron emission tomography for detection of bone marrow involvement in children and adolescents With Hodgkin's Lymphoma, J. Clin. Oncol. 29 (2011) 3523–3528.

[41] P. Duffy, K. Ecklund, MR features of primary bone lymphoma in children, Pedia Radio. 53 (2023) 2400–2410, https://doi.org/10.1007/s00247-023-05772-w.

[42] A. Rosolen, S.L. Perkins, C.R. Pinkerton, R.P. Guillerman, J.T. Sandlund, C. Patte, A. Reiter, M.S. Cairo, Revised interntional pediatric non-hodgkin lymphoma staging system, J. Clin. Oncol. 33 (18) (2015 Jun 20) 2112–2118.

[43] J. Mhlanga, A. Alazraki, S. Cho, H. Lai, H. Nadel, H. Pandit-Taskar, J. Qi, D. Rajderkar, S. Voss, P. Watal, K. McCarten, Imaging recommendations in pediatric lymphoma: a COG diagnostic imaging committee/SPR oncology committee white paper, Pedia Blood Cancer 70 (Suppl 4) (2023) e29968.

[44] R. Haupt, M. Minkov, I. Astigarraga, E. Schäfer, V. Nanduri, R. Jubran, R.M. Egeler, G. Janka, D. Micic, C. Rodriguez-Galindo, S. Van Gool, J. Visser, S. Weitzman, J. Donadieu, Euro Histio Network. Langerhans cell histiocytosis (LCH): Guidelines for diagnosis, clinical work-up, and treatment for patients till the age of 18 years, Pedia Blood Cancer 60 (2013) 175–184, https://doi.org/10.1002/pbc.24367.

[45] H.W. Goo, D.H. Yang, Y.S. Ra, J.S. Song, H.J. Im, J.J. Seo, T. Ghim, H.N. Moon, Whole-body MRI of Langerhans cell histiocytosis: comparison with radiography and bone scintigraphy, Pedia Radio. 36 (10) (2006) 1019–1031.

[46] J.R. Kim, H.M. Yoon, A.Y. Jung, Y.A. Cho, J.J. Seo, J.S. Lee, Comparison of whole-body MRI, bone scan, and radiographic skeletal survey for lesion detection and risk stratification of Langerhans Cell Histiocytosis, Sci. Rep. 9 (2019) 317, https://doi.org/10.1038/s41598-018-36501-1.

[47] A. Perrone, K. Lakatos, F. Pegoraro, I. Trambusti, I. Fotzi, V. Selvi, H. Prosch, F. Sertorio, U. Pötschger, C. Favre, M. Conte, M. Minkov, E. Sieni, Whole-body magnetic resonance imaging for staging Langerhans cell histiocytosis in children and young adults, Pedia Blood Cancer 70 (2) (2023) e30064, https://doi.org/10.1002/pbc.30064. Epub 2022 Nov 1. PMID: 36317710.

[48] S. Jessop, D. Crudgington, K. London, S. Kellie, R. Howman-Giles, FDG PET-CT in pediatric Langerhans cell histiocytosis, Pedia Blood Cancer 67 (1) (2020) e28034.

[49] J. Ferrell, S. Sharp, A. Kumar, M. Jordan, J. Picarsic, A. Nelson, Discrepancies between F-18-FDG PET/CT findings and conventional imaging in Langerhans cell histiocytosis, Pedia Blood Cancer 68 (4) (2021) e28891.

[50] J.M. Maris, M.D. Hogarty, R. Bagatell, S.L. Cohn, Neuroblastoma, Lancet 369 (23) (2007) 2106–2120.

[51] C. Chung, T. Boterberg, J. Lucas, J. Panoff, D. Valteau-Couanet, B. Hero, R. Bagatell, C.E. Hill-Kayser, Neuroblastoma, Pedia Blood Cancer 68 (Suppl 2) (2021) e28473, https://doi.org/10.1002/pbc.28473. PMID: 33818884; PMCID: PMC8785544.

[52] T.A. Vik, T. Pfluger, R. Kadota, V. Castel, M. Tulchinsky, J.C. Farto, S. Heiba, A. Serafini, S. Tumeh, N. Khutoryansky, A.F. Jacobson, 123)I-mIBG scintigraphy in patients with known or suspected neuroblastoma: Results from a prospective multicenter trial, Pedia Blood Cancer 52 (7) (2009 Jul) 784–790, https://doi.org/10.1002/pbc.21932. PMID: 19185008.

[53] A. Samim, G.A.M. Tytgat, G. Bleeker, S.T.M. Wenker, K.L.S. Chatalic, A.J. Poot, N. Tolboom, M.M. van Noesel, M.G.E.H. Lam, B. de Keizer, Nuclear medicine imaging in neuroblastoma: current status and new developments, J. Pers. Med 11 (4) (2021) 270, https://doi.org/10.3390/jpm11040270. PMID: 33916640; PMCID: PMC8066332.

[54] A. Samim, T. Blom, A.J. Poot, A.D. Windhorst, M. Fiocco, N. Tolboom, A.J.A. T. Braat, S.L.M. Viol, R. van Rooij, M.M. van Noesel, M.G.E.H. Lam, G.A.M. Tytgat, B. de Keizer, 18F]mFBG PET-CT for detection and localisation of neuroblastoma: a prospective pilot study, Eur. J. Nucl. Med Mol. Imaging 50 (4) (2023) 1146–1157, https://doi.org/10.1007/s00259-022-06063-6.

[55] L. Borgwardt, J.S. Brok, K.F. Andersen, J. Madsen, N. Gillings, M.Ø. Fosbøl, C. L. Denholt, P.S. Wehner, L.H. Enevoldsen, P. Oturai, D. Czyzewska, H. H. Johannesen, L. Højgaard, I.N. Petersen, L.S. Sørensen, C. Schulze, E.S. Saxtoft, F. L. Andersen, B.M. Fischer, 18F]mFBG long axial field of view PET-CT without general anaesthesia reveals concise extension of neuroblastoma in a 9-month-old boy, Eur. J. Nucl. Med Mol. Imaging 50 (8) (2023) 2563–2564, https://doi.org/10.1007/s00259-023-06160-0. Epub 2023 Feb 28. PMID: 36849749; PMCID: PMC10250494.

[56] K.K. Matthay, V. Edeline, J. Lumbroso, M.L. Tanguy, B. Asselain, J.M. Zucker, D. Valteau-Couanet, O. Hartmann, J. Michon, Correlation of early metastatic response by 123I-metaiodobenzylguanidine scintigraphy with overall response and event-free survival in stage IV neuroblastoma, J. Clin. Oncol. 21 (2003) 2486–2491.

[57] G.A. Yanik, M.T. Parisi, B.L. Shulkin, A. Naranjo, S.G. Kreissman, W.B. London, J. G. Villablanca, J.M. Maris, J.R. Park, S.L. Cohn, P. McGrady, K.K. Matthay, Semiquantitative MIBG scoring as a prognostic indicator in patients with stage 4 neuroblastoma: a report from the Children's oncology group, J. Nucl. Med 54 (2013) 541–548.

[58] V. Lewington, B. Lambert, U. Poetschger, Bar Sever, Z. Giammarile, F. McEwan, A. J.B. Castellani, R. Lynch, T. Shulkin, B. Drobics, M. Staudenherz, A. Ladenstein, R. I-mIBG scintigraphy in neuroblastoma: development of a SIOPEN semi-quantitative reporting, method by an international panel, Eur. J. Nucl. Med Mol. Imaging 44 (2017) 234–241.

[59] I.S.A. de Vries, R. van Ewijk, L.M.E. Adriaansen, A.E. Bohte, A.J.A.T. Braat, R. D. Fajardo, L.S. Hiemcke-Jiwa, M.L.F. Hol, S.A.J. Ter Horst, B. de Keizer, R.R. G. Knops, M.T. Meister, R.A. Schoot, L.E. Smeele, S.T. van Scheltinga, B. Vaarwerk, J.H.M. Merks, R.R. van Rijn, Imaging in rhabdomyosarcoma: a patient journey, Pedia Radio. 53 (4) (2023) 788–812, https://doi.org/10.1007/s00247-023-05596-8. Epub 2023 Feb 27.

[60] K.A. Bailey, L.H. Wexler, Pediatric rhabdomyosarcoma with bone marrow metastasis, Pedia Blood Cancer 67 (5) (2020) e28219, https://doi.org/10.1002/pbc.28219. Epub 2020 Feb 26.

[61] D. Huang, P. Watal, D. Drehner, D. Dhar, T. Chandra, Rhabdomyosarcoma with diffuse bone marrow metastases, Cureus 14 (2) (2022) e21863, https://doi.org/10.7759/cureus.21863 eCollection 2022 Feb.

[62] M. Scheer, T. Dantonello, P. Brossart, D. Dilloo, L. Schweigerer, S. Feuchtgruber, M. Sparber-Sauer, C. Vokuhl, S.S. Bielack, T. Klingebiel, E. Koscielniak, T. von Kalle, Cooperative Weichteilsarkom Studiengruppe (CWS). Importance of whole-body imaging with complete coverage of hands and feet in alveolar rhabdomyosarcoma staging. Cooperative Weichteilsarkom Studiengruppe (CWS), Pedia Radio. 48 (5) (2018) 648–657, 10.1007/s00247-017-4066-8. Epub 2018 Jan 24.

[63] F. Mercolini, P. Zucchetta, N. Jehanno, N. Corradini, R.R. Van Rijn, T. Rogers, A. Cameron, G. Scarzello, B. Coppadoro, V. Minard-Colin, S. Gallego, J. Chisholm, J.H. Merks, G. Bisogno, Role of 18F-FDG-PET/CT in the staging of metastatic rhabdomyosarcoma: a report from the European paediatric Soft tissue sarcoma Study Group, Eur. J. Cancer 155 (2021) 155–162, https://doi.org/10.1016/j.ejca.2021.07.006.

[64] P.G. Casali, S. Bielack, N. Abecassis, H.T. Aro, S. Bauer, R. Biagini, S. Bonvalot, I. Boukovinas, J.V.M.G. Bovee, B. Brennan, T. Brodowicz, J.M. Broto, L. Brugières, A. Buonadonna, E. De Álava, A.P. Dei Tos, X.G. Del Muro, P. Dileo, C. Dhooge, M. Eriksson, F. Fagioli, A. Fedenko, V. Ferraresi, A. Ferrari, S. Ferrari, A.M. Frezza, N. Gaspar, S. Gasperoni, H. Gelderblom, T. Gil, G. Grignani, A. Gronchi, R.L. Haas, B. Hassan, S. Hecker-Nolting, P. Hohenberger, R. Issels, H. Joensuu, R.L. Jones, I. Judson, P. Jutte, S. Kaal, L. Kager, B. Kasper, K. Kopeckova, D.A. Krákorová, R. Ladenstein, A. Le Cesne, I. Lugowska, O. Merimsky, M. Montemurro, B. Morland, M.A. Pantaleo, R. Piana, P. Picci, S. Piperno-Neumann, A.L. Pousa, P. Reichardt, M. H. Robinson, P. Rutkowski, A.A. Safwat, P. Schöffski, S. Sleijfer, S. Stacchiotti, S. J. Strauss, K. Sundby Hall, M. Unk, F. Van Coevorden, W.T.A. van der Graaf, J. Whelan, E. Wardelmann, O. Zaikova, J.Y. Blay, ESMO Guidelines Committee, PaedCan and ERN EURACAN. Bone sarcomas: ESMO-PaedCan-EURACAN clinical practice guidelines for diagnosis, treatment and follow-up, Ann. Oncol. 29 (2018) iv79–iv95.

[65] Z. Pennington, A.K. Ahmed, E. Cottrill, E.M. Westbroek, M.L. Goodwin, D. M. Sciubba, Systematic review on the utility of magnetic resonance imaging for operative management and follow-up for primary sarcoma-lessons from extremity sarcomas, Ann. Transl. Med 7 (10) (2019) 225, https://doi.org/10.21037/atm.2019.01.59.

[66] M.J. Thompson, J.C. Shapton, S.E. Punt, C.N. Johnson, E.U. Conrad 3rd, MRI identification of the osseous extent of pediatric bone sarcomas, Clin. Orthop. Relat. Res 476 (3) (2018) 559–564, https://doi.org/10.1007/s11999.0000000000000068.

[67] J.C. Davis, N.C. Daw, F. Navid, C.A. Billups, J. Wu, A. Bahrami, J.J. Jenkins, S. E. Snyder, W.E. Reddick, V.M. Santana, M.B. McCarville, J. Guo, B.L. Shulkin, 18F-FDG uptake during early adjuvant chemotherapy predicts histologic response in pediatric and young adult patients with Osteosarcoma, J. Nucl. Med 59 (1) (2018) 25–30, https://doi.org/10.2967/jnumed.117.190595.

[68] D.S. Hawkins, S.M. Schuetze, J.E. Butrynski, J.G. Rajendran, C.B. Vernon, E. U. Conrad, 3rd, J.F. Eary, 18F]Fluorodeoxyglucose positron emission tomography predicts outcome for Ewing sarcoma family of tumors, J. Clin. Oncol. 23 (34) (2005) 8828–8834, https://doi.org/10.1200/JCO.2005.01.7079.

[69] B.H. Byun, C.B. Kong, I. Lim, B.I. Kim, C.W. Choi, W.S. Song, W.H. Cho, D.G. Jeon, J.S. Koh, S.Y. Lee, S.M. Lim, Early response monitoring to neoadjuvant chemotherapy in osteosarcoma using sequential ^{18}F-FDG PET/CT and MRI, Eur. J. Nucl. Med Mol. Imaging 41 (8) (2014) 1553–1562.
[70] H.M. Fuglø, S.M. Jørgensen, A. Loft, D. Hovgaard, M.M. Petersen, The diagnostic and prognostic value of 18F-FDG PET/CT in the initial assessment of high-grade bone and soft tissue sarcoma. A retrospective study of 89 patients, Eur. J. Nucl. Med Mol. Imaging 39 (2012) 1416–1424.
[71] A.H. Behzadi, S.I. Raza, J.A. Carrino, C. Kosmas, A. Gholamrezanezhad, K. Basques, G.R. Matcuk, Jr, J. Patel, H. Jadvar, Applications of PET/CT and PET/MR imaging in primary bone malignancies, PET Clin. 13 (2018) 623–634, https://doi.org/10.1016/j.cpet.2018.05.012.
[72] A. Saifuddin, B. Sharif, I. Oliveira, S. Kalus, J. Barnett, I. Pressney, The incidence of skip metastases on whole bone MRI in high-grade bone sarcomas, Skelet. Radio. 49 (6) (2020) 945–954, https://doi.org/10.1007/s00256-019-03369-9. Epub 2020 Jan 9.
[73] L. Kager, A. Zoubek, U. Kastner, B. Kempf-Bielack, J. Potratz, R. Kotz, G.U. Exner, C. Franzius, S. Lang, R. Maas, H. Jürgens, H. Gadner, S. Bielack, Cooperative Osteosarcoma Study Group. Skip metastases in osteosarcoma: experience of the Cooperative Osteosarcoma Study Group, J. Clin. Oncol. 24 (10) (2006) 1535–1541, https://doi.org/10.1200/JCO.2005.04.2978.
[74] K.M. Ingley, S. Wan, S. Vöö, R. Windsor, M. Michelagnoli, A. Saifuddin, S. J. Strauss, Is it time to call time on bone marrow biopsy for staging ewing sarcoma (ES)?, Published online 2021 Jun 29, Cancers (Basel) 13 (13) (2021 Jul) 3261, https://doi.org/10.3390/cancers13133261.
[75] K. Park, H. Kim, K.N. Koh, H.J. Im, Y.U. Cho, S. Jang, E.J. Seo, C.J. Park, Bone marrow findings in patients with ewing sarcoma/primitive neuroectodermal tumor, Published online 2021 Sep 1, Ann. Lab Med 41 (5) (2021) 499–501, https://doi.org/10.3343/alm.2021.41.5.499.
[76] A. Gupta, R.F. Riedel, C. Shah, S.C. Borinstein, M.S. Isakoff, R. Chugh, J. M. Rosenblum, E.S. Murphy, S.R. Campbell, C.M. Albert, S. Zahler, S.M. Thomas, M. Trucco, Consensus recommendations in the management of Ewing sarcoma from the National Ewing Sarcoma Tumor Board, Cancer 129 (21) (2023) 3363–3371, https://doi.org/10.1002/cncr.34942. Epub 2023 Jul 5.
[77] M. Kunstreich, S. Kummer, H.J. Laws, A. Borkhardt, M. Kuhlen, Osteonecrosis in children with acute lymphoblastic leukemia, Haematologica 101 (2016) 1295–1305.
[78] S.C. Kaste, E.J. Karimova, M.D. Neel, Osteonecrosis in children after therapy for malignancy. AJR, Am. J. Roentgenol. 196 (2011) 1011–1018, https://doi.org/10.2214/AJR.10.6073.
[79] H.E. Daldrup-Link, T. Henning, T.M. Link, MR imaging of therapy-induced changes of bone marrow, Eur. Radio. 17 (2007) 743–761.
[80] A.T. Trout, S.E. Sharp, B.K. Turpin, B. Zhang, M.J. Gelfand, Optimizing the interval between G-CSF therapy and F-18 FDG PET imaging in children and young adults receiving chemotherapy for sarcoma, Pedia Radio. 45 (2015) 1001–1006.